Robotics and Computer-Integrated Manufacturing 27 (2011) 949–962

Contents lists available at ScienceDirect

Robotics and Computer-Integrated Manufacturing

journal homepage: www.elsevier.com/locate/rcim

Design and development of automatic visual inspection system for PCB manufacturing

N.S.S. Mar, P.K.D.V. Yarlagadda *, C. Fookes

School of Engineering Systems, Queensland University of Technology, George Street 2, Brisbane QLD 4001, Australia

ARTICLE INFO

Article history:
Received 30 June 2010
Received in revised form
30 November 2010
Accepted 14 March 2011
Available online 7 April 2011

Keywords:
Automatic PCB inspection
Segmentation of solder joint
Classification of solder joint
Log-Gabor filter
Classifier fusion

ABSTRACT

Inspection of solder joints has been a critical process in the electronic manufacturing industry to reduce manufacturing cost, improve yield, and ensure product quality and reliability. This paper proposes two inspection modules for an automatic solder joint classification system. The "front-end" inspection system includes illumination normalisation, localisation and segmentation. The "back-end" inspection involves the classification of solder joints using the Log-Gabor filter and classifier fusion. Five different levels of solder quality with respect to the amount of solder paste have been defined. The Log-Gabor filter has been demonstrated to achieve high recognition rates and is resistant to misalignment. This proposed system does not need any special illumination system, and the images are acquired by an ordinary digital camera. This system could contribute to the development of automated non-contact, non-destructive and low cost solder joint quality inspection systems.

1. Introduction

Assembly of Printed Circuit Boards (PCBs) using Surface Mount Technology (SMT) has been widely used in the electronic industry recently [1]. As a result, the electronic components rely on the solder joint to provide the electrical connection to the PCBs; therefore, the quality of the solder joint can be critical to the quality of the electronic components [2]. Automatic Optical Inspection (AOI) of solder joints has been a critical issue for quality control in PCB assembly as AOI has the enormous potential of completely automating human visual inspection procedures [3,4].

Automated solder joint inspection requires the extraction of information from the solder joint surface [5]. However, the specularity of the solder joint surface causes difficulties in the automated extraction of relevant information. Specular reflections of the solder joint surface may appear or disappear with small changes in viewing direction. A specular surface is often illuminated at a distance by a point light source, which prevents ideal smooth shading that matches its shape for the effective classification of solder joints. Furthermore, the shape of the solder joints tend to vary greatly with soldering conditions including the amount of solder paste and heating level applied during the soldering process. As a consequence, the variety of the solder joint shapes is also a barrier to the development of an automatic solder joint inspection system. Furthermore, the variety of components on the board and the sophisticated layout of the board introduce more complexity for solder joint inspection, which makes the development of automated pattern recognition systems for this purpose a non-trivial task. The aim of these inspection procedures is to detect and locate any potential solder joint defects, which will impede or break down the functions of the final PCB products. Common solder joint defects which are of concern include: no solder, opens, shorts, and bridges [6].

In this study, a computer vision system is proposed for the automatic detection, localisation, segmentation and classification of solder joints on PCBs under different illumination conditions. This paper introduces a new technique for solder joint defect classification using the Log-Gabor filter and classifier fusion which has been demonstrated to achieve a high recognition rate and is resistant to misalignment. Further testing demonstrates the advantage of the Log-Gabor filter over both Discrete Wavelet Transform (DWT) and Discrete Cosine Transform (DCT).

The outline of this paper is as follows. Section 2 will provide an overview of existing inspection techniques in the field. Section 3 will present the research methodology, the segmentation of the solder joint inspection system and experimental results on PCB images. The classification of solder joint defects and experimental results will be described in Section 4. In Section 5, the performance of the classifier fusion is evaluated. Lastly, the paper is concluded in Section 6.

2. Literature review

In commercial PCB assembly processes, solder joint inspection has one essential problem for quality control in the PCBs.

* Corresponding author.
E-mail address: y.prasad@qut.edu.au (P.K.D.V. Yarlagadda).

0736-5845/$ - see front matter © 2011 Elsevier Ltd. All rights reserved.
doi:10.1016/j.rcim.2011.03.007

For accurate visual inspection, it is necessary to obtain the system that is resistant to variation of light and requires robust algorithms for classification. Moreover, classification criteria for solder joints are usually based on human experience and can be changed according to the products. To overcome these limitations, complex image acquisition systems that need special illumination systems and several kinds of inspection algorithms are developed.

2.1. Illumination design

The imaging of solder joints is a difficult task in automated visual inspection technology due to the specularity of the solder joint surface. Reflections of the specular solder joint may appear or disappear even with small changes in viewing direction [5]. Moreover, specular surfaces rarely exhibit smooth shading that matches its shape, which makes it complex to recognise a specular surface from visual information. The different shapes of solder joints are also an obstacle to develop an automatic solder joint inspection system. The shape of the solder joints tends to vary with soldering conditions. Even those classified into the same type of solder joints are slightly different in shape when carefully examined. To overcome this problem, several researchers have tackled it by using a dedicated illumination system, which can maintain sufficient illumination levels to reveal the darker regions of the solder joint image.

Bartlet et al. [7] used four overhead fluorescent lamps and one fluorescent ring lamp to effectively inspect solder joints and avoid shadows in the captured image. Capson and Eng [8] used a tiered-colour illumination method to generate colour contours onto the solder joints. This illumination system consisted of red and blue circular fluorescent lamps with different heights. By examining the contour shape measured by geometric descriptors, solder joint defects could be determined. The lighting arrangement allowed direct correlation between the solder joint profile and colour planes. The colours of the lights also aided in segmentation of the solder joints from the PCBs.

Kim et al. [5,9] improved the previous system by using three colour circular lamps (Red, Green, Blue) with different illumination angles. Three different types of image were sequentially captured as three layers of lights were turned on one after another and obtained 2D and 3D features of the images. An attractive approach for an illumination system was developed by using only one layer of tiered light and two features [10]. Insufficient, acceptable and excess solder joints were classified by two straight lines on the 2D feature plane. The number of circular illuminations can be reduced to one when the incident angle was optimised. This method significantly saved time for image scanning and computation compared to previous illumination systems. However, the processing of colour images required very high over-heads in terms of computation and complex processing.

Meanwhile, a hemispherical lighting system with a structured LED array was developed with a CCD camera to take grey-level images sequentially [1]. The structured LED array was placed on the lighting system to project light from different positions onto the solder joint surface. A slant map was used to extract information from the images based on the slant angles which represented the solder joint shape and were directly relative to the quality of the solder joint. This system achieved a 7.69% overall false alarm ratio.

Ong et al. [11] combined orthogonal and oblique grey-level images with the use of two viewing direction configurations, namely, the orthogonal view and oblique view. For orthogonal images, a camera was set up perpendicular to the plan of the PCBs. A viewing direction inclined approximately 40° to the vertical plan was used for oblique images. However, it was important to maintain high accuracy of the relative geometrical position of the cameras for a multiple camera setup. Belbachir [12] used a simple method to capture images by using one CCD camera. The acquisition system was covered by a black screen and the PCB was illuminated by fluorescent lamps. This setting helped to control the illumination condition by avoiding an external light source.

2.2. Classifier design

In order to complete the inspection system, classifiers have been developed using different approaches to select features extracted from an image. A pattern recognition system classifies solder joints based upon statistics obtained from a "training set" of each solder joint's class. The Bayesian and maximum likelihood classifier are a traditional statistical approach for classification [7]. In this approach it is necessary to have knowledge on the probability distribution of each class and this requires a large number of experiments. Bartlett et al. [7] used a minimum classifier to classify each solder joint into one of the two good types and seven defected types depending on five different features.

Rule based classification systems have been widely used in machine learning applications because of their easy to understand ability and interpretability. In some cases, this method needs counter measures against the appearance of unexpected members of a class. Capson and Eng [8] proposed a tree classifier by using geometric descriptors, which measure the shape of the contours and the colour level intensities of the solder joint images. For board 'A', 93.5% of solder joints were correctly identified and for board 'B', a 76% success rate was achieved. The false alarm rates were 3.0% and 4.3%, respectively. Another rule based classification system was also employed by using fuzzy set theory [2,13]. This can be especially useful when objects are not clearly members of one class or another. In addition, fuzzy techniques specify to what degree the object belongs to each class, which is useful information in solder joint recognition.

In recent years, Artificial Neural Network (ANN) approaches have been applied to AOI systems due to their learning capability and nonlinear classification performance. ANNs can be divided into the unsupervised ANNs and the supervised ANNs. Multilayer neural networks are one of the supervised neural networks and have been applied to solder joint inspection. Kim et al. [5] proposed the neural network with two following modules: a processing module and training module. The first module was designed to implement the calculation of the correlations in functional terms and the second module was designed to learn about solder joint classification as a human inspector. The advantage of a multilayered neural network is the ability to learn human experiences. However, the complexity of solder joint shapes causes the neural network's convergence rate to degrade.

The other neural network approach is an unsupervised neural network such as a Learning Vector Quantisation (LVQ) neural network [14]. The LVQ method is good for pattern classification because of their fast learning nature, reliability and convenience of use. One disadvantage for LVQ is that it cannot sometimes produce a correct decision for complex classification problems. Kim and Cho [14] applied an adaptive learning mechanism to correct the LVQ classifier. The adaptive learning mechanism can select the optimal number of prototypes set to achieve performance within an acceptable error rate. Again, Ong et al. [11] proposed a new approach using a dual viewing angle imaging method with an ANN and learning vector quantisation architecture. From the experimental results, this system had an improved recognition rate and resistance to noise. However, high accuracy on the relative geometrical position of the camera was required.

In order to improve the human knowledge in the classification of complex solder joint criteria, Ko et al. [15] combined a fuzzy logic scheme into the LVQ neural network. In the neural network module, three LVQ classifiers were used to cluster solder joints by using similarity between an input pattern and prototype patterns. In the fuzzy module, new classification criteria were generated using a pre-defined rule built by the inspectors. More accurate classification results were achieved because expert knowledge was applied into the classification criteria.

Accianni et al. [16,17] extracted two feature vectors, the "geometric" feature vector and the "wavelet" feature vector, from the images and used a multiple neural network system to characterise solder joint defects on PCBs. Two feature vectors feed the multiple neural network system constituted by two MultiLayer Perceptron neural networks and the LVQ network for the classification. From the experimental results, the multiple neural network system achieved the best compromise in terms of recognition rate and time with respect to the single MLP and LVQ network.

Another technique included an ANN ensembles based machine vision inspection system [18]. This system used a Genetic Algorithm to train many one layered perceptrons respectively as classifiers which were combined linearly into an ensemble. To correct the trained ANN's errors, the weights of training samples were adjusted by the AdaBoost algorithm. Meanwhile, many works and various techniques have been developed to classify the solder joint defects. Kim et al. [9] developed a two stage classifier to recognise four types of solder joints: good, insufficient, excess and no solder joints. In the first stage, MultiLayer Perceptrons were used to roughly classify the image by the evaluation of 2D simple features. For some uncertain results, 3D features were classified based on the Bayes classifier.

The Support Vector Machine (SVM) was also developed to inspect the solder joint quality [19]. The SVM produced a good classification result even with a small size of training data due to its ability to maximise the distance between each class. Jiang et al. [6] introduced a simpler method to identify the position of the solder joint and a tree structure classifier to categorise the solder joint defects. This methodology did not require special lighting or special equipment to capture the PCB image. A Pareto chart was also used to observe the average distance of different types of solder joints with respect to the various features, i.e. binary image-based features and grey value-based feature. On-line 3D PCB is inspected by the application of phase profilometry [38]. It is a new phase extraction algorithm for 3D optical profilometry based on the projection of a periodic light pattern and phase measurement.

2.3. Knowledge gap

Many researchers have developed complex image acquisition systems that need specially tailored illumination devices. In practice it is far too time-consuming and cost ineffective to conduct comprehensive studies on illumination and specular reflections of solder joints. In order to use a simple hardware setup and no special lighting, one of the solutions is to conduct research on effective illumination normalisation algorithms.

Furthermore, most of the methods described above utilise neural networks for image processing. The advantage of a classifier using a neural network is the ability to learn human experiences, but the disadvantage is when the input data space is too complex to determine decision boundaries for effective classification. The performance of the classifier may degrade due to the inability of the neural network to process complex input variables. Statistical approaches such as Bayesian and maximum likelihood classifiers require knowledge on the probability distribution of data, which demand a large number of experiments to be conducted. A rule based method has an advantage in using human skill to make classifications. But for the appearance of unexpected members that are not included in the construction rule, this method requires several measurements. Due to these reasons, the existing methods may not give ideal results when inconsistent solder joint shapes are encountered. In summary, most of the research which has been conducted on solder joint inspection require a robust method for the classification algorithm.

3. Research methodology for automated inspection system

This section will outline the inspection procedure involved in the automatic vision-based inspection system for solder joint classification. There are four main tasks in solder joint classification: image capture, segmentation, feature extraction and classification. Several inspection algorithms have been applied for each task. Fig. 1 represents the detailed methodology for the solder joint defect classification system proposed by this research. The first step is acquisition of the image. The image acquired by the camera contains the components and solder joints to be classified and other irrelevant zones within the image. Thus, the important Region of Interest (ROI) must be extracted from the acquired image. To extract the ROI, the Hough Transform is utilised for automatic alignment of the PCB. Afterwards an illumination normalisation technique is applied to an image, which effectively eliminates the effects of uneven lighting conditions. Following this, the image is transformed from an RGB to a YIQ colour model for the effective detection of solder joints from the background. This is then followed by thresholding, region filling and segmentation of solder joints.

The next step of the diagnosis process is the feature extraction. In this step, features are extracted by three different methods: Log-Gabor filter, Discrete Cosine Transform (DCT) and Discrete Wavelet Transform (DWT). Finally, these features are measured by Mahalanobis Cosine distance and five types of solder joints are classified. These include: good solder joint, excess solder joint, less solder joint, no solder joint and bridge solder joint. The method for combining information is examined to improve the accuracy and robustness for the classification of solder joints.

3.1. Hough transform

The Hough transform is a powerful method for detecting edges [21]. It transforms between the Cartesian space and a parameter space in which a straight line can be defined. The advantage of the Hough transform is that the pixels lying on one line need not all be contiguous. This method is very useful when trying to detect lines with short breaks in them due to noise, or when objects are partially occluded. For this reason, the Hough transform technique is used to locate the PCB so that the PCB does not need to be placed onto a precision X–Y table. In this way the PCB can be located on an automatic conveyor line, without interrupting the line production. This algorithm also helps to improve the accuracy of the solder joint segmentation.

The Hough Transform method has been recognised as one of the most popular methods to extract parameterised lines from an image. The transform maps a line in the image space (x,y) into a point in the Hough Transform parameter space. For straight line detection, the equation of a line can be expressed as,

$$\rho = x\cos(\theta) + y\sin(\theta). \quad (1)$$

Figs. 2 and 3 show the image before and after applying the Hough transform technique. The figures clearly show how the image has been rotated to ensure that the PCB is correctly oriented in the horizontal and vertical directions.

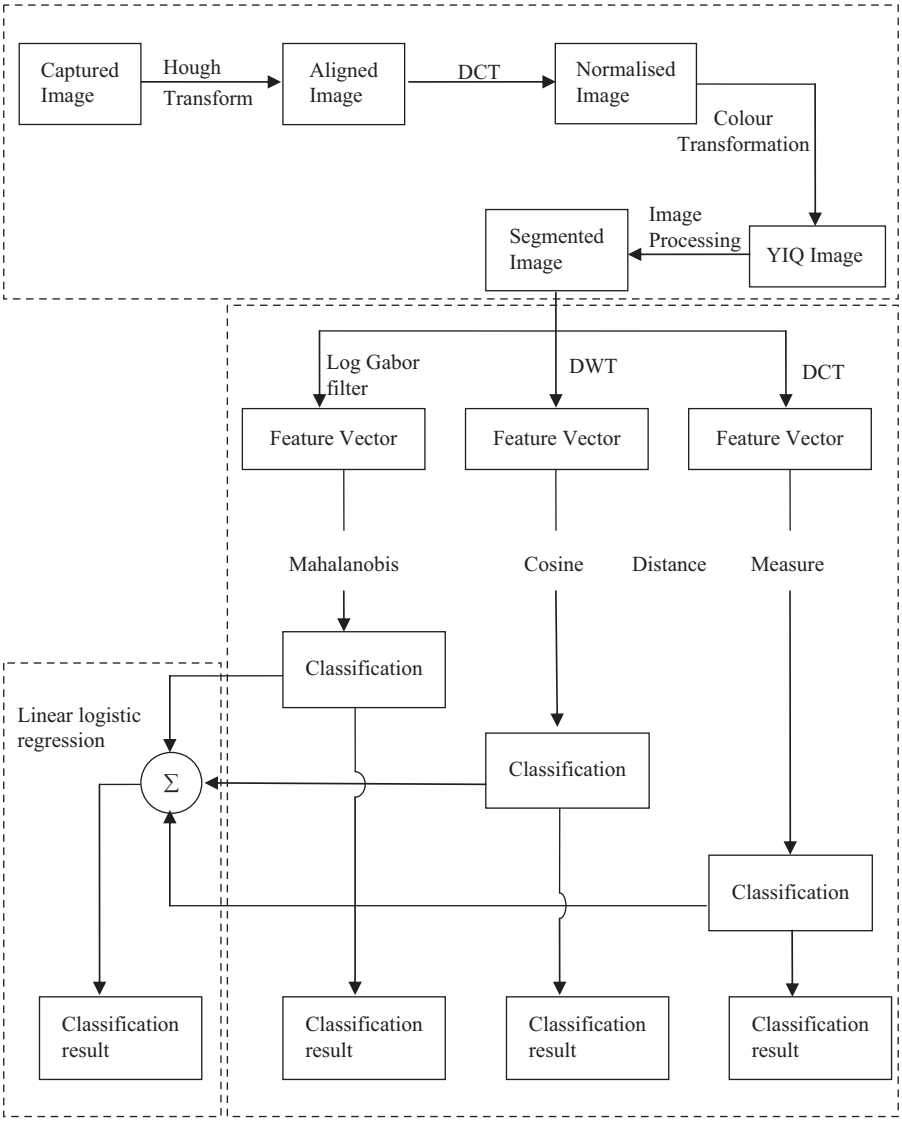

Fig. 1. Inspection procedure.

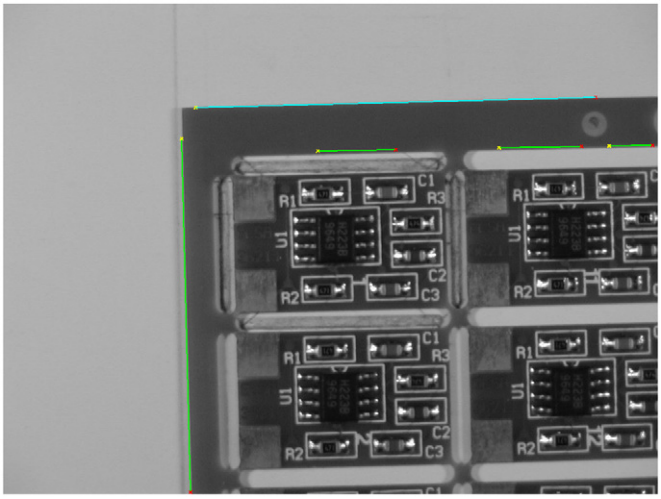

Fig. 2. Acquired image.

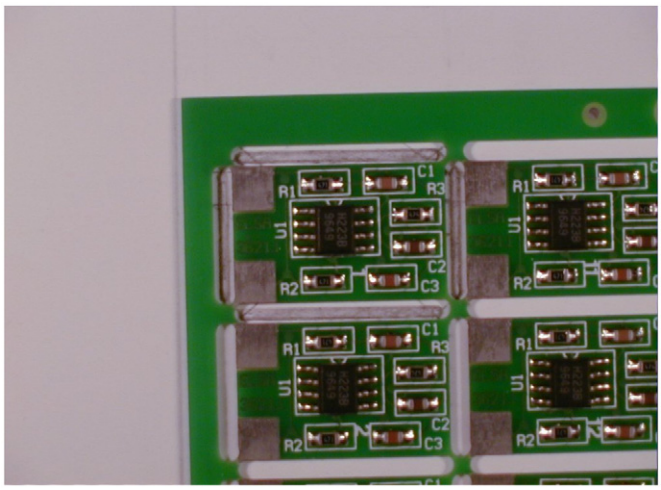

Fig. 3. Result of Hough transform.

3.2. Illumination normalisation

Since solder joint images are highly variant with illumination variation, it results in a challenge for this research. The same solder joint can appear greatly different under varying lighting conditions. There is a need to normalise an image under different lighting. In this approach, images are normalised using the Discrete Cosine Transform (DCT) technique to normalise the images to appear stable under different lighting conditions. A useful aspect of the DCT is the ability to physically interpret the basic functions. The position of the coefficient reflects the corresponding sum of pixel values in the block. The 0th coefficient represents the lowest frequency band in DCT. Since illumination variations mainly lie in the low-frequency band, an appropriate number of DCT coefficients are truncated to minimise variations under different lighting conditions [20]. There are four established types of Discrete Cosine Transforms (DCT's), i.e., DCT-I, DCT-II, DCT-III and DCT-IV. DCT-II is more widely applied in signal coding. The 2D $M \times N$ DCT is defined as [20],

$$C(u,v) = \alpha(u)\alpha(v)\sum_{x=0}^{M-1}\sum_{y=0}^{N-1} f(x,y)\cos\left[\frac{\pi(2x+1)u}{2M}\right]\cos\left[\frac{\pi(2y+1)v}{2N}\right], \quad (2)$$

and the inverse transform is defined as

$$f(x,y) = \sum_{u=0}^{M-1}\sum_{v=0}^{N-1} \alpha(u)\alpha(v)C(u,v)\cos\left[\frac{\pi(2x+1)u}{2M}\right]\cos\left[\frac{\pi(2y+1)v}{2N}\right], \quad (3)$$

where

$$\alpha(u) = \begin{cases} \frac{1}{\sqrt{M}}, & u=0 \\ \sqrt{\frac{2}{M}}, & u=1,2,\ldots,M-1 \end{cases}, \quad \alpha(v) = \begin{cases} \frac{1}{\sqrt{N}}, & v=0 \\ \sqrt{\frac{2}{N}}, & v=1,2,\ldots,N-1 \end{cases}.$$

In the proposed approach, the DCT is performed on the entire image to obtain all the frequency components of the image.

This block matrix consists of DCT coefficients, C_{uv}. The top-left coefficient, C_{00} is correlated to the low frequencies of the original image block. As C_{00} is removed, the DCT coefficients correlate to higher and higher frequencies of the image block, where C_{uv} corresponds to the highest frequency. It is important to eliminate the low frequency, which is the most sensitive to the human eye. The manner of discarding DCT coefficients is shown in Fig. 4.

As illustrated in Figs. 5 and 6, the original image is improved by applying the DCT for illumination normalisation.

3.3. Colour transformation

It is not easy to separate the solder joints and other background information from a PCB image as there are many lines and markings that have similar values as the solder joint [6]. In this case, the PCB image is transformed from an RGB colour model to YIQ colour model. The advantages of the YIQ colour model are: (1) processing the Y component only will differ from unprocessed image in its appearance of brightness and (2) most high frequency components of a colour image are in Y. The image is transformed to YIQ, which gives one luminance signal Y and two colour signals I&Q. Again, I stands for in-phase, while Q stands for quadrature, referring to the components used in quadrature amplitude modulation [22]. Eq. (4) describes the transformations between the RGB and YIQ colour spaces,

$$\begin{bmatrix} Y \\ I \\ Q \end{bmatrix} = \begin{bmatrix} 0.2290 & 0.5870 & 0.1140 \\ 0.5957 & -0.2744 & -0.3213 \\ 0.2115 & -0.5226 & 0.3111 \end{bmatrix} \begin{bmatrix} R \\ G \\ B \end{bmatrix}. \quad (4)$$

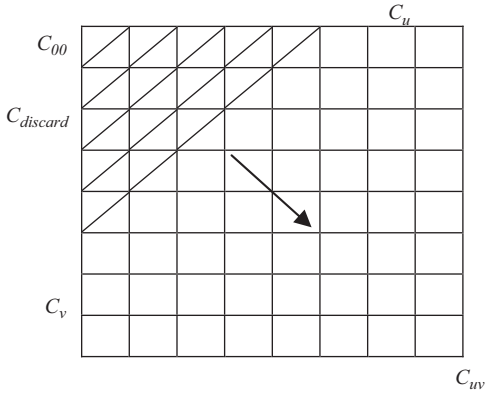

Fig. 4. Manner of discarding DCT coefficients (only the first 8×8 coefficients are shown).

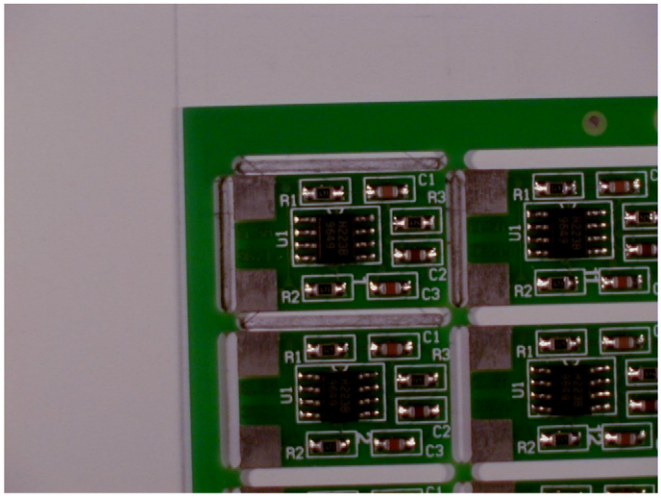

Fig. 5. Original image.

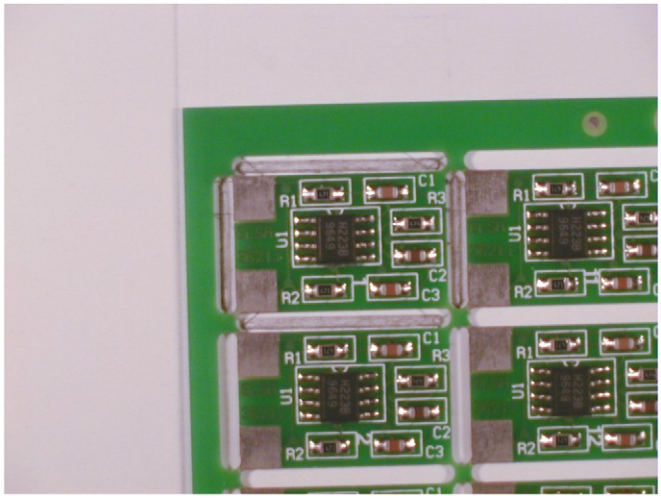

Fig. 6. Reconstructed image by applying the DCT.

3.4. Segmentation of solder joints

3.4.1. Thresholding

After performing the colour transformation of an image, a solder joint needs to be extracted from its background by a threshold selection. If the object has a different average grey level from that of

its background, it is often difficult to select an appropriate threshold. In this research, a successive iterative process is described to achieve an optimum threshold [23]. The histogram of an image is initially segmented into two parts using a starting threshold value such as half the maximum dynamic range. Then, the sample data are computed into two classes, which are the sample mean of the grey values associated with the foreground pixels and the sample mean of the grey values associated with the background pixels. Then a new threshold value is computed as the average of the above two sample means. The resultant threshold and its upper and lower thresholds are applied to the PCB image. Then the new threshold value is calculated according to the number of components detected. This process is repeated until the number of components does not change any more.

3.4.2. Region filling

Although the solder joints have been detected, closed or opened holes might occur on solder joints after segmentation because of the surface property and shape of solder joints [2]. These holes can be confusing when determining the solder joint location. Consequently these holes need to be mended. Firstly, erosion and dilation via morphology is applied to enclose an opened hole. If dilation of Morphology is used to enclose a hole, it might change the original shape of the solder joints. In that case, Region Filling is applied to mend these closed holes. Region Filling is based on set dilations, complementation, and intersections [24]. In Fig. 7 "*A*" denotes a set containing a subset whose elements are 8-connected boundary points of a region.

Beginning with a point p inside the boundary, the objective is to fill the entire region with 1's. The following equation is used to fill the region with 1's:

$$X_k = (X_{k-1} \oplus B) \cap A^c \quad k = 1,2,3,\ldots, \tag{5}$$

where $X_0 = p$, and B is the symmetric structuring element. The algorithm terminates at iteration step k if $X_k = X_{k-1}$. The set union of X_k and A contains the filled set and its boundary. The result of region filling is shown in Fig. 8.

3.4.3. Segmentation process

There are two stages in the segmentation process. In the first stage of segmentation, components are extracted from the acquired image and the next step is to extract an image of the solder joint from each component. In performing the first step of segmentation, the pixels which represent components and background are grouped into meaningful regions [25]. The white pixels correspond to components and black pixels correspond to background. Once an object pixel is found, the entire connected object region is enumerated. Finally, the centroid of the region is calculated as a simple measure of object location. Fig. 9 illustrates the output of applying the segmentation on the PCB board by defining the boundary around the components.

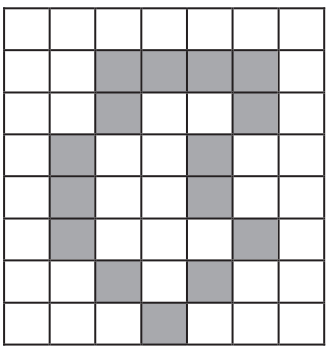

Fig. 7. Set *A*.

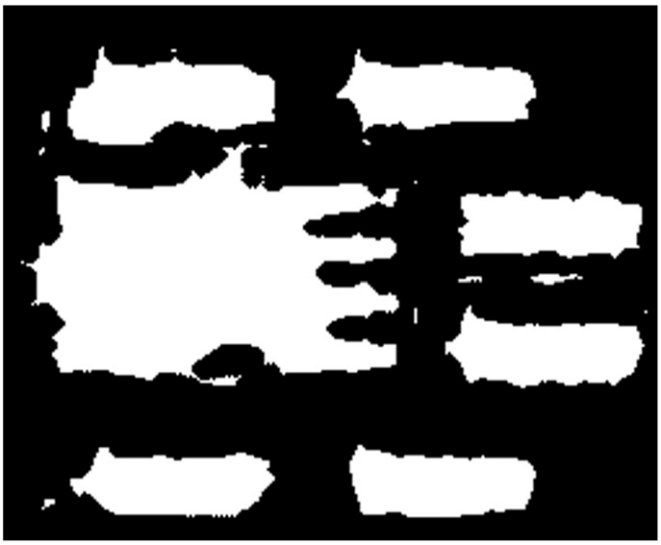

Fig. 8. Result of region filling.

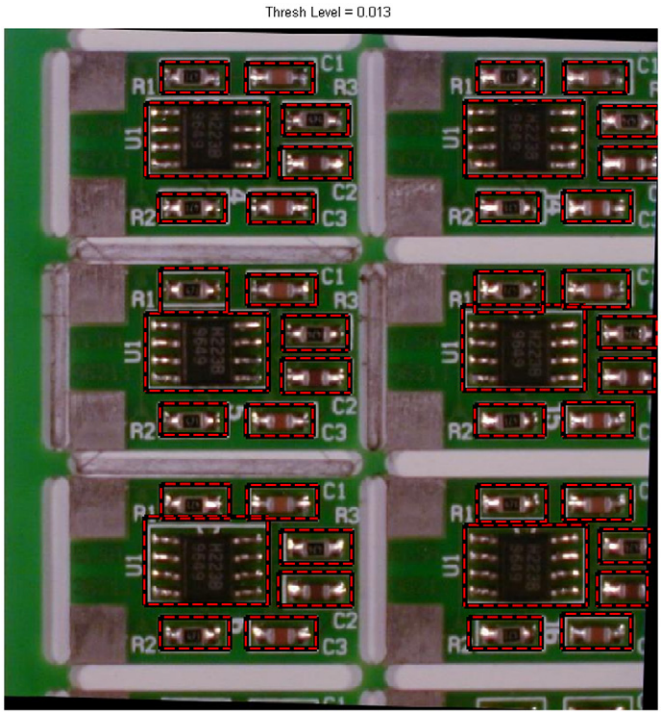

Fig. 9. An example of detected components from database 1.

For the next step of segmentation, each solder joint can be isolated by projection of the image horizontally and vertically. Each lead–pad pair can be isolated by vertical projection and the solder region can be identified be by horizontal projection (i.e. Fig. 10). Suppose $p \times m$ is a matrix associated with the thresholded image. The equations for the horizontal projection H and the vertical projection V are defined as follows:

$$H = \sum_{i=1}^{p} \rho_i, \tag{6}$$

and

$$V = \sum_{j=1}^{m} \gamma_j, \tag{7}$$

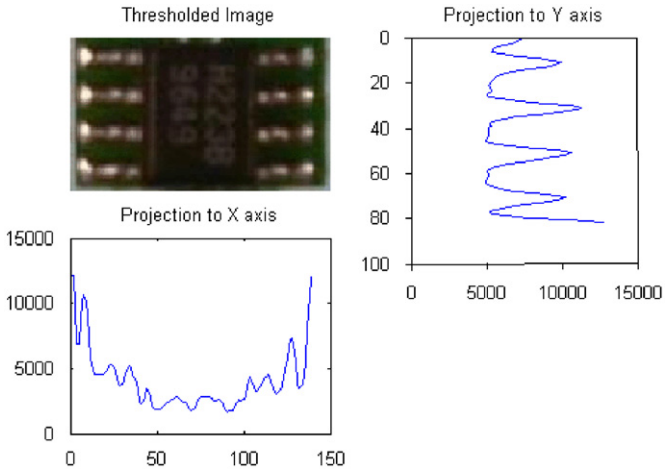

Fig. 10. Image processing of solder joint.

Fig. 11. An example of detected solder joints from database 1.

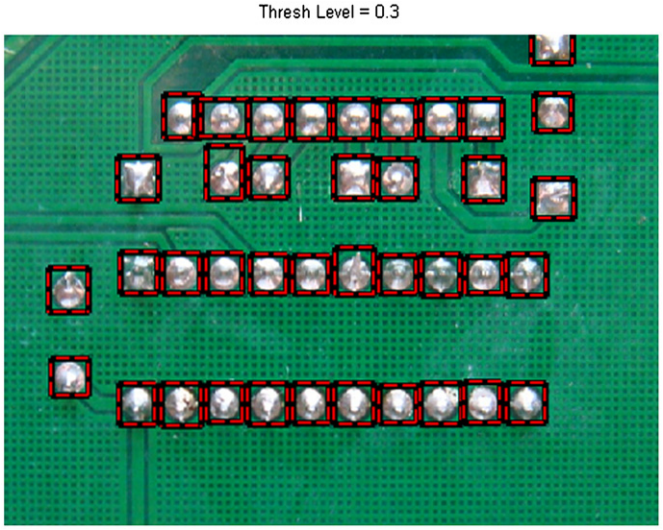

Fig. 12. An example of detected solder joints form database 2.

where ρ_i and γ_j are the i-th row and j-th column of the image, respectively.

Figs. 11 and 12 show examples of detected solder joints from database 1 and database 2.

3.5. Databases

A number of datasets have been used to evaluate the methodologies and hypotheses laid out in this paper. They are Database 1, Database 2 and Database 3. Each of the databases have a different number of subjects and acquisitions, in addition there are imaging conditions, which are particular to each database. Database 1 is supported by Ahmed Nabil Belbachir (Vienna University of Technology). In this image acquisition system, an *XY* positioning system controls all the displacements of the CCD camera [12]. The dimension of the framed region is controlled by modifying the lens zooming. In order to control the illumination conditions, the acquisition system is covered with black screens that avoid external light sources. The circuit under test is illuminated using commercial fluorescence lamps. Database 1 is utilised for testing of the automatic segmentation of solder joints.

Database 2 is supported by MRD Rail Technologies and the PCB images are captured by a standard digital camera under a fluorescent light source in the lab. There are no special illumination systems or advanced *X–Y* positioning systems. Database 2 is especially used for testing segmentation. Since the height of the camera from the image is inconsistent, when acquiring the image, it is not suitable to use in classification.

Due to the above challenges, the acquisition system for image Database 3 is fixed at a certain height. The acquiring system for image database 3 is constituted by a digital camera mounted on a fixed position and acquires images of the PCB under test. This acquisition system does not require special illumination systems or advanced *X–Y* position systems.

3.6. Experimentation and result analysis

Two sets of solder joint databases, (1) and (2), are used in the experiments. The total of 3840 (database 1) and 621 (database 2) solder joints are used in these experiments. The parameter such as the size of solder joints is approximately defined. Three indices are used to evaluate the segmentation results:

- Hit rate: percentage of correctly detected joints.
- Miss rate: percentage of undetected joints.
- False alarm rate: percentage of incorrectly detected joints.

Four different types of experiments have been performed on solder joint images to identify the best segmentation algorithm. The first experiment is conducted with the combination of two algorithms: normalisation illumination and automatic thresholding. The second experiment is performed for automatic thresholding without illumination normalisation. The third and fourth experiments are performed for manual thresholding with and without illumination normalisation. The manual threshold value is selected by plotting the resultant thresholding value from automatic thresholding and selecting its mean value. The results of the test stage are summarised in Tables 1 and 2 for databases 1 and 2.

Table 1 represents the segmentation results based on database 1. There are 36 PCB images in this database, which contain 3840 sold joints altogether. In the first condition of the experiment, 99.93% of solder joints are successfully detected with 0.07% of miss rate and 0% of false alarm rate. The second condition of experiment does not include the illumination normalisation step. The performance of segmentation slightly decreases to 99.70% in hit rate and slightly increases to 0.3% in miss rate. But the false rate remains the same as the test condition 1. In manual thresholding with illumination normalisation, 97.56% of hit rate, 2.23% of miss rate and 0.21% of false alarm rate are achieved. Comparing the results for manual thresholding without illumination normalisation, it is clear that the detection rate declines to 78.94%, the miss rate and false alarm rate increase to 20.91% and 0.15%, respectively, in test condition 4. Therefore, it is easily apparent that the combination of automatic thresholding and illumination normalisation achieved the best result.

Table 1
The segmentation result for database 1.

Condition of experiment	Hit rate (%)	Miss rate (%)	False rate (%)
(1) Automatic thresholding with illumination normalisation	**99.93**	**0.07**	**0**
(2) Automatic thresholding without illumination normalisation	99.70	0.3	0
(3) Manual thresholding with illumination normalisation	97.56	2.23	0.21
(4) Manual thresholding without illumination normalisation	78.94	20.91	0.15

Table 2
The segmentation result for database 2.

Condition of experiment	Hit rate (%)	Miss rate (%)	False rate (%)
(1) Automatic thresholding with illumination normalisation	**99.83**	**0.17**	**0**
(2) Automatic thresholding without illumination normalisation	99.03	0.64	0.24
(3) Manual thresholding with illumination normalisation	96.62	3.38	0
(4) Manual thresholding without illumination normalisation	81.64	18.04	0.32

Table 2 represents the segmentation results based on database 2. There are 38 PCB images in this database, which contain 621 solder joints altogether. As in database 1, automatic thresholding with illumination normalisation achieved highest detection with 99.83% of hit rate, 0.17% of miss rate and 0% of false alarm rate. The hit rate decreases to 99.03%, miss rate and false rate increase to 0.64% and 0.24%, respectively, when illumination normalisation is removed from the experiment. In manual thresholding with illumination normalisation, 96.62% of hit rate, 3.38% of miss rate and 0% of false rate are achieved. The correct detection rate is low for manual thresholding without illumination normalisation with 81.64% of hit rate, 18.04% of miss rate and 0.32% of false alarm rate.

Since the acquisition system for databases 1 and 2 are not the same, the detection results for both databases are slightly different. In order to control the illumination condition in database 1, the acquisition system is covered with black screens that help to avoid external light sources. Database 2 is captured by a standard digital camera under a fluorescent light source in the lab. There are no special illumination systems or advanced X–Y position systems. From both databases, it can be clearly seen that illumination normalisation improves the segmentation in both automatic thresholding and manual thresholding. For database 1, the hit rate increases from 99.70% to 99.93% in automatic thresholding and the hit rate rises from 78.94% to 97.56% in manual thresholding. The segmentation result for database 2 also improves in the same way. The hit rate increases by 0.8% for automatic thresholding and 14.98% for manual thresholding.

Subsequently, the automatic thresholding performance significantly improves the detection of the solder joint. For both databases 1 and 2, the hit rate increases from 97.56% to 99.93% and from 96.62% to 99.83% when normalisation illumination is employed. Similarly, the hit rate increases from 78.94% to 99.7% and from 81.64% to 99.03% when normalisation illumination is not performed on the solder joint image. As a result, the experimental results on these two databases show that segmentation performance can be significantly improved when both illumination and automatic thresholding are employed.

4. Classification of solder joints

This section examines a new technique for solder joint defect classification using the Gabor filter, which has been demonstrated to achieve high recognition rates and is resistant to misalignment [27]. This filter has also found favour in many image processing fields due to its desirable characteristic of spatial locality and orientation selectivity. The use of Log-Gabor features has been set as a method for more accurately representing the shape information in solder joint image [28].

The Discrete Wavelet Transform (DWT) is also applied to extract feature vectors from the solder joint image. The advantage of the wavelet is that it can be treated as an image-to-image transformation. This will enable each wavelet coefficient to be treated as a pixel image and thus allows the image difference operation to be carried out [29]. In addition, the Discrete Cosine Transform (DCT) has an energy compaction property and achieves good performance in illumination normalisation so the DCT is also applied for the feature extraction of solder joint images.

Five different levels of solder joint quality with respect to the amount of solder pasted have been classified utilising the Mahalanobis Cosine distance measure. The five types of solder joints include: good solder joint, excess solder joint, less solder joint, no solder joint and bridge solder joint. The experimental results are devoted to comparing the recognition performance of the Log-Gabor filter, DWT and DCT. The results prove that the Log-Gabor filter is the best compromise in terms of correct classification percentage and cost. In addition, the features utilised for diagnosis are evaluated without the knowledge of the industrial physical parameter process which is the advantage of using the Log-Gabor filter in this research.

4.1. Gabor and Log-Gabor filter

An important property of the Gabor filter is that it has optimal localisation properties in both the spatial and frequency domain [30]. A two-dimensional Gabor filter consists of a sinusoidal plane of the particular frequency and orientation modulated by a two dimensional Gaussian envelope. The two main components of the Gabor filter are the complex sinusoidal carrier $s(x)$ and the Gaussian envelope $\omega_r(x)$. These components are expressed as

$$s(x) = \exp\{2\pi j k^T x\}, \tag{8}$$

where $k=[v_0 v_0 \omega_0]$ defines the spatial frequency of the complex valued plane wave and

$$\omega_r(x) = K\exp\{-\pi(\alpha^T[R_\theta(x-x_0)]^2\}, \tag{9}$$

where K is a scaling factor, $\alpha=[\sigma_1^2\sigma_2^2\ldots\sigma_N^2]^T$ the variance of the Gaussian and x_0 is the spatial coordinates of the peak. The R_θ is a rotation of the Gaussian about its centre.

The Gabor filter bank is a well known technique to determine a feature domain for the representation of an image. The Gabor filter bank can be designed by varying the spatial frequency and orientation of the Gabor filter, which mimics a band-pass filter.

However, the Gabor filter can be designed for a bandwidth of 1 octave maximum with a small DC component in the filter. To overcome this limitation, Field [31] proposes the Log-Gabor filter. The Log-Gabor filter has no DC component and can be constructed with any arbitrary bandwidth. The frequency response of the Log-Gabor filter is defined as

$$\Phi(\omega) = \exp - \frac{\ln(\omega/\omega_0)^2}{2\ln(\sigma/\omega_0)^2}, \tag{10}$$

where ω_0 is the centre frequency of the sinusoid and σ is a scaling factor of the bandwidth.

There are two important characteristics in the Log-Gabor filter. Firstly the Log-Gabor filter function always has zero DC components, which contribute to improve the contrast ridges and edges of images. Secondly, the Log-Gabor function has an extended tail at the high frequency end, which allows it to encode images more efficiently than the ordinary Gabor function. The Log-Gabor filter has a Gaussian transfer function when viewed on a logarithmic frequency scale instead of a linear scale.

In this experiment, the Log-Gabor filter bank is constructed with a total of 6 orientations and 5 scales. The shape parameter, σ/ω_0 is chosen such that each filter had a bandwidth of approximately 1.5 octaves. A total of 30 feature vectors representing different scales and orientations are achieved.

4.2. Discrete wavelet transform

Wavelet decomposition is the projection onto an orthonormal set of basis vectors which are generated by dilation translation of a single "mother wavelet." The simplest mother wavelet is the Haar wavelet,

$$\psi(t) = \begin{cases} 1: & 0 \le t < 1/2 \\ -1: & 1/2 \le t < 1 \\ 0: & \text{else} \end{cases}, \tag{11}$$

which generates the basis set,

$$\left\{ \psi_{j,n}(t) = \frac{1}{\sqrt{2^j}} \psi\left(\frac{t - 2^j n}{2^j} \right) \right\}_{(j,n) \in Z^2}.$$

The "mother wavelet" has low-pass and high-pass responses. At each application of the filters, the signal is split into a low and high frequency component, which are then down sampled by a factor of two to give a consistent memory requirement regardless of decomposition level. This also allows the same filters to be used at each level as they have effectively been upscaled by a factor of two.

Fig. 13 illustrates the first three levels of the 2D wavelet transform applied to a good solder joint image. At each level, the approximation of the previous level is split into horizontally, vertically and diagonally filtered images along with a subsequent approximation image. This multilevel representation can be coerced into a filter bank form by grouping the detail coefficients together at each level. In the following experimentation, 3 levels of decomposition are employed to achieve the equivalent of 4 filter banks.

There are many popular wavelet families being used in different applications such as Daubechies and Coiflet wavelets. The equal error rate (EER) of the Daubechies wavelet transform (level 2) is 5% and the EER of the Daubechies wavelet (level 4) is slightly more than 5%. However, they have the disadvantage of being more computationally expensive than the Haar wavelets. The Haar wavelet transform has a number of advantages:

- It is conceptually simple.
- It is fast.
- It is memory efficient, since it can be calculated in place without a temporary array.

In this experiment, the Haar wavelet provides the best performance across all images when compared to the other wavelet families.

4.3. Discrete cosine transform

The Discrete Cosine Transform (DCT) has been widely used in feature extraction and image compression because it has the effect of concentrating the energy in a signal in a relatively small number of coefficients [32]. In order to construct filter-banks from a DCT representation, the common overlapping block implementation, as is used in the Part-Face method of Lucey and Chen [33] and Sanderson and Paliwal [34], is utilised. A detected and normalised image is divided into blocks of $N \times N$ pixels size. In this experiment, $M=N$ and $N=8$. Each block, $f(x,y)$, where $x,y=0,1, \ldots, N-1$, is decomposed in terms of pre-defined orthogonal 2D DCT basis functions as in Fig. 14. The result is a $N \times N$ coefficient matrix $C(u,v)$

$$C(u, v) = \alpha(u)\alpha(v) \sum_{x=0}^{N-1} \sum_{y=0}^{N-1} f(x,y) \cos\left[\frac{\pi(2x+1)u}{2M} \right] \cos\left[\frac{\pi(2y+1)v}{2N} \right], \tag{12}$$

where $u,v=0,1,\ldots,N-1$, $\alpha(v)=1/N$ for $v=0$, $\alpha(v)=2/N$ for $v=1,2,\ldots,N-1$.

The top-left DCT coefficient is removed from the representation since it only represents the average intensity value of the block. From the remaining DCT coefficients the ones containing the highest information are extracted via a zig-zag pattern as in Fig. 15.

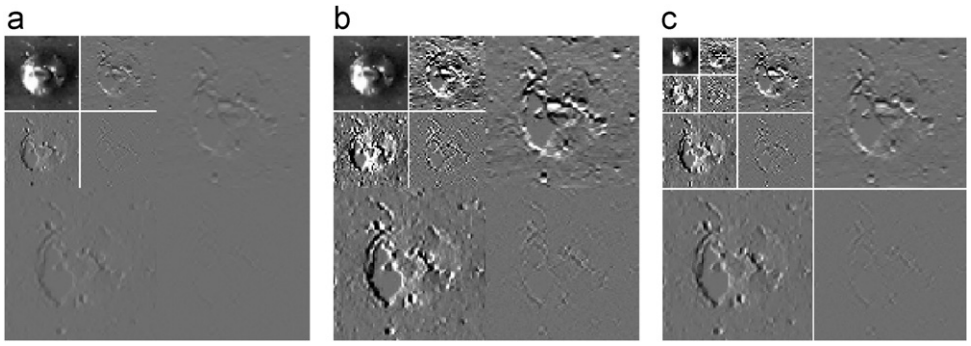

Fig. 13. First three levels of DWT using Haar wavelet: (a) first level, (b) second level and (c) third level.

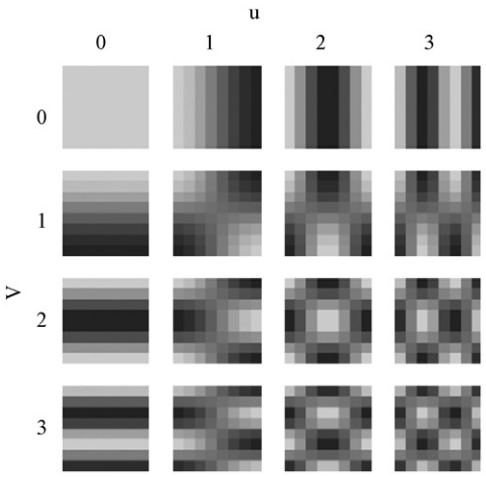

Fig. 14. Graphical interpretation of the first few 2D DCT basic function for $N=8$ (lighter colours represent larger value).

	0	**1**	**2**	**3**
0	0	1	5	6
1	2	4	7	12
2	3	8	11	13
3	9	10	14	15

Fig. 15. Ordering of 2D DCT coefficients $C(v,u)$ for $N_P=4$.

For a block located at (b,a), the 2D DCT feature vector is composed of

$$\vec{x} = \left[c_0^{(b,a)} \quad c_1^{(b,a)} \quad \cdots \quad c_{M-1}^{(b,a)} \right]^T, \tag{13}$$

where $c_n^{(b,a)}$ denotes the nth 2D DCT coefficient and M is the number of retained coefficients. To ensure adequate representation of the image, each block overlaps its neighbouring blocks horizontally and vertically by 50% [35]. Thus for an image which has N_Y rows and N_X columns, there are $N_D=(2(N_Y/N_P)-1)\times(2(N_X/N_P)-1)$ blocks.

4.4. Distance measure

The Mahalanobis Cosine Distance is used to compute the similarity measure between two filter banks. Many experimental results have shown that the Mahalanobis Cosine Distance measure provides better performance than many other distance measures [27]. The transformation between the image space and the Mahalanobis space is needed to be performed before computing the Mahalanobis Cosine distance. The Mahalanobis space is defined as a space where the sample variance along each dimension is one. To transform into Mahalanobis space, each coefficient in the image space feature vector is divided by its corresponding standard deviation. Let u and v be two vectors in the Eigenspace and σ is the standard deviation of the i-th dimension. Let m and n be the corresponding vectors in the Mahalanobis space. The relationship between the vectors is defined as

$$m_i = \frac{u_i}{\sigma_i} \quad \text{and} \quad n_i = \frac{v_i}{\sigma_i}. \tag{14}$$

The Mahalanobis Cosine Distance measure is the cosine of the angle between the projection of the images on the Mahalanobis space. So, for images u_i and v_i with corresponding projections m and n in Mahalanobis space, the Mahalanobis Cosine Distance is

$$D_{\text{Mahcosine}(u,v)} = -\frac{|m||n|\cos\theta_{mn}}{|m||n|} = -\frac{m\cdot n}{|m||n|}. \tag{15}$$

4.5. The detection error trade-off curve

The verification results are presented using Detection Error Trade-off (DET) plots. The DET plot has a logarithmic scale on both axes, which makes it easier to observe the system contrast since the curves tend to be close to linear. The DET curve plot highlights the trade-off between false acceptance rate (false alarm probability) and false rejection rate (miss probability), which is useful in areas where the trade-off between the two error types are important. The false acceptance rate is the measurement of the probability that a system will incorrectly indentify a solder joint class as another. The false rejection rate is the measurement of the probability that a system will fail to identify a solder joint class which is properly defined. There are a number of operating points on the curve, which typically need to be considered in verification of the performance. The most common is the Equal Error Rate (EER). The EER is the point at which the false alarm rate is equal to the miss probability rate. This may be used in applications to find the point of minimum cost in each type of error. The smaller the EER, the better the performance of the recognition system. However, in general the whole DET curve is considered.

4.6. Experimentation and result analysis

Image database 3 is used to evaluate the classification algorithm. The resolution of each solder joint image after segmentation is 40×40 pixels. Fig. 16 shows the five different types of solder joints after segmentation. For each type of solder joint, 50 images are used as the training samples and two hundred images are used as the test samples. The images used for training and testing sets have been chosen randomly from the original database for every individual experiment. During testing, experiments are performed 25 times and the value averaged to get one complete classification result. When the number of experiments reaches 25, the mean value becomes stable and this value is used to plot the graph. The experimental result is plotted as a probability distribution and results are evaluated by DET plots. From 1000 test images, the solder joints are classified into five different groups with respect to the amount of solder paste: good, excess, less, bridge and no solder joints. All the experiments and results are performed on the existing database and the result might be varied when this method is applied to an actual production environment. Other types of defects can be added to the system.

A good classification algorithm has a low false alarm probability and miss probability, which equates to a small EER rate. In Table 3, the training samples are shown by column and the testing samples are shown by row. The diagonal values across the table represent the recognition rate for the classification of solder joints and the rest are EERs. For example, from the reading across the first row and the first column, we see the percentage of good joints correctly classified was 97.0%. The next column represents EER (3%) of excess solder joints classified as good solder joints. Since good joints have already been detected, it is not necessary to include them in the classification of the individual defect types. From the table, the recognition rates for good solder joints, excess solder joints and bridge solder joints are relatively high with a

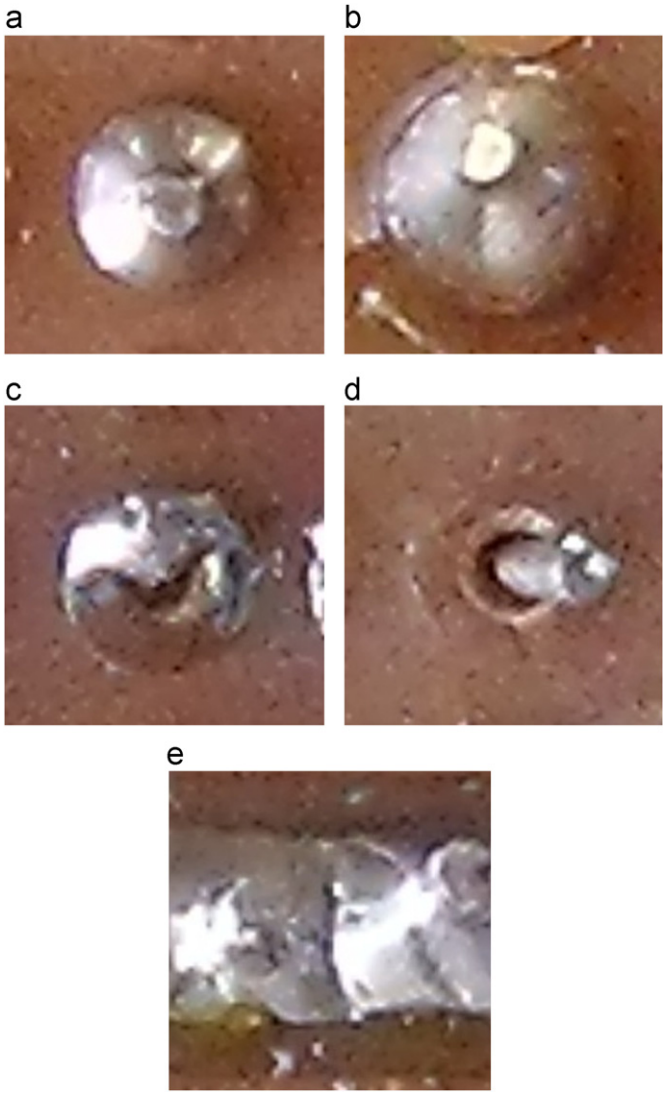

Fig. 16. Different types of solder joint appearance.

Table 3
Summary result for recognition rate of solder joints across five categories by using Log-Gabor filter.

Solder joint types	Recognition rate and EER for Gabor filter				
	G	*E*	*L*	*N*	*B*
G (Good Joint)	**97**	3	4.5	1	0.5
E (Excess Joint)	–	**97**	2	4	1.5
L (Less Joint)	–	32	**60**	40	3.5
N (No Joint)	–	14	9	**90**	1
B (Bridge Joint)	–	7	0.5	0	**96.5**

recognition rate of approximately 97% each. The recognition rate of no solder joint is 90%, while the recognition rate achieved for less solder joint is 60%. An EER of less than 5% is achieved for miss-classification as good solder joint, excess solder joint and bridge solder joint as other defect types except for a 7% EER, which is achieved from miss-classification of excess solder joint as bridge solder joint, which can be found in rows 1(G), 2(E) and 5(B) of the table. The EER is higher for miss-classification as no solder joint and less solder joint. The highest EER is 40% for no solder joint incorrectly classified as less solder joint. The performance degradation is due to the high degree of difference between individual less solder joint images and the limitation of the Log-Gabor filter, which is discussed below. The recognition performance can be improved further through classifier fusion.

The proposed algorithm achieves good performance because the Log-Gabor filter can capture visual properties such as spatial localisation, orientation selectivity, and spatial frequency characteristics. Log-Gabor functions have no DC component, which contributes to the improvement to the contrast ridges and edges of images. Moreover, they have an extended tail at the high frequency end, which enables them to obtain wide spectral information with localised spatial extent and consequently helps to preserve true ridge structures of images. Because of the above characteristics, the Log-Gabor filters give an average correct classification rate about 88%. Although the overall results are promising, the results presented in the table indicate that some deterioration of the recognition results is observed for the less and no solder joint defects because of the unstable surface of those defects.

The unstable surfaces are caused because of the following reasons in the Log-Gabor filter bank. In the Log-Gabor filter bank, its elementary functions overlap each other introducing coefficient redundancy between neighbouring coefficients. Due to non-orthogonality there is no straight forward method of finding the parameter values of the Log-Gabor filter. The parameter values depend upon the surface (its orientation and frequency of repetition of the surface pixels), which is to be identified by a particular set of the Log-Gabor filter. If any of these are affected due to different image degradation and the distortions of images, then the Log-Gabor filter bank may not even work well.

In some cases, the Gabor filter bank cannot discriminate a certain image as a whole but rather certain frequencies from the image. This problem appears when image surfaces share the same frequencies or are comprised of close frequencies for certain orientations. These indicate that different feature selection strategies would have to be implemented to achieve a better classification result. As a result, DWT and DCT are studied to minimise the error in the Log-Gabor filter.

In Table 4, the diagonal values across the table represent the recognition rate for each type of solder joint and the rest represent the EER using the DWT. A percentage of 96% of good joints are correctly classified, which is the same as the percentage of bridge solder joints correctly classified. This is followed by the percentage of correct classification of no solder joint and excess joint with 90% and 86%. Only 65% of less solder joints are correctly classified. The average percentage of the correct classifications varied across different types from 96% to 65%, whereas the DWT yields an average correct classification rate about 86%.

Although the overall recognition rate achieved is not as high as the Log-Gabor filter, the DWT perform swell in less solder joint defects where the recognition rates increase by 5% compared to the Log-Gabor filter. The EERs of less solder joint classified as no solder joint and no solder joint classified as less solder joint are

Table 4
Summary result for recognition rate of solder joints across five categories by using wavelet transform.

Solder joint types	Recognition rate and ERR for wavelet transform				
	G	*E*	*L*	*N*	*B*
G (Good Joint)	**96**	10	5	1.5	0.5
E (Excess Joint)	–	**86**	12	16	5
L (Less Joint)	–	20	**65**	>40	8
N (No Joint)	–	5	>40	**90**	16
B (Bridge Joint)	–	4	2	4	**96**

about 40% due to the high degree of difference between each solder joint and the limitation of the Haar wavelet transform.

Since the Haar wavelet transform performs an average and difference on a pair of values and then shifts over by two values and calculates another average and difference on the next pair, it cannot detect if a big change takes place from an odd index value to an even index value. For example, for a one dimensional signal that has 24 elements as shown in Fig. 17, there is a large drop between elements 6 and 7, and a large rise between elements 11 and 12. After the first stage of the wavelet transform, the result for the high frequency computation is shown in the figure as well. Only the large drop between elements 6 and 7 is detected in Fig. 17d_1. The large rise between elements 11 and 12 is not detected because the change is from an odd element to an even element. For this reason, a performance degradation arises for certain types of images like less solder joints.

In Table 5, the diagonal values across the table represent the recognition rate for each type of solder joint and the rest represent the EER using the DCT. The number of good joints and bridge joints correctly classified is 95%, the number of excess joints classified as a good joint is 7%, the number of less joints classified as good joint is 8% and so on. Similarly, the number of excess joints correctly classified is 93%. The average percentage of correct classifications varied across the different types from 95% to 60%. An average correct classification rate achieved using the DCT is 80.6%. Although the overall recognition rate achieved is not as high as the Log-Gabor filter, the DCT is evaluated as a method

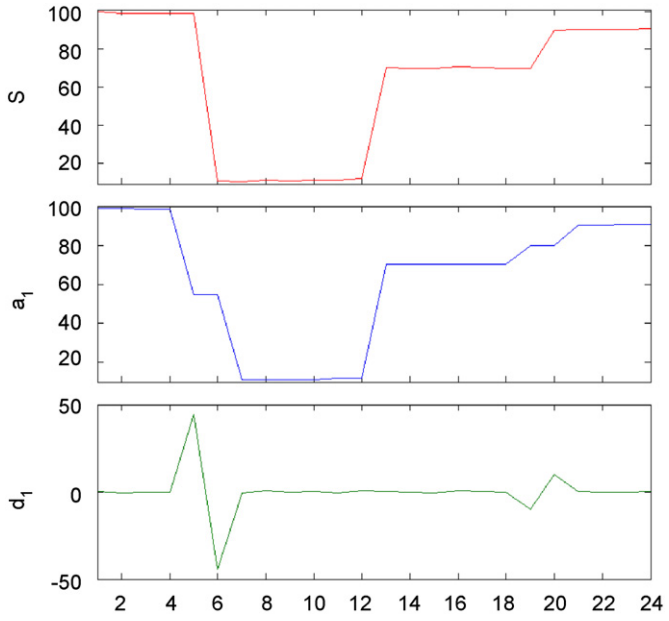

Fig. 17. One dimensional signal with a large drop between elements 6 and 7 and a large rise between elements 11 and 12.

Table 5
Summary result for recognition rate of solder joints across five categories by using discrete cosine transform.

Solder joint types	Recognition rate and ERR for discrete cosine transform				
	G	*E*	*L*	*N*	*B*
G (Good Joint)	**95**	7	8	1	1
E (Excess Joint)	–	**93**	9	3	10
L (Less Joint)	–	> 40	< **60**	40	33
N (No Joint)	–	> 40	> 40	< **60**	15
B (Bridge Joint)	–	7	1	1	**95**

Table 6
Summary result for recognition rate of solder joints across five categories by using classifier fusion.

Solder joint types	Recognition rate and EER for classifier fusion				
	G	*E*	*L*	*N*	*B*
G (Good Joint)	**98.5**	2	2	1	0.5
E (Excess Joint)	–	**98.5**	2	0.5	1.5
L (Less Joint)	–	6.5	**70**	23	2
N (No Joint)	–	3	7	**95**	1
B (Bridge Joint)	–	3	0.5	0	**98.5**

for utilisation in classifier fusion. From the experimental results, the Log-Gabor representation outperforms both the DWT and DCT representations and all methods can be fused together to obtain desirable characteristics of all. (Table 6)

The recognition rate of less and no solder joints achieved is approximately 60% due to the high degree of difference between each solder joint and the limitation of the DCT. The blockwise DCT process destroys the invariance properties of the system, because the blockwise frequencies do not produce a simple relation to the frequencies achieved by just transforming the image into the frequency domain. Hence, any linear scaling factor from the time domain will not carry over into the frequency domain if blocking is used because linearity is no longer maintained. For this reason, the performance degradation is caused for certain types of images like less solder joints and no solder joints.

5. Classifier fusion

In this section, a method for combining the information from these classification systems is examined. Fused classification aims to improve the accuracy and robustness of a classification system by combining multiples sources of information. These information sources need to be complementary as redundant information will not improve verification. Classifier fusion combines the information from multiple verification systems that are achieved from three different classifiers. The advantage of the linear classifier fusion technique is that complex data and feature normalisation methods do not need to be employed.

This research aims to improve solder joint classification by performing linear classifier score fusion. Linear classifier score fusion is chosen as it has been shown to be robust to estimation error [36]. A weighted linear fusion (where the optimal weights are found) using a linear logistic regression (*llr*) is employed in this research. The weighted fusion is of the form

$$C_{Weight\_sum} = \sum_{k=1}^{M} \beta_k C_k, \tag{16}$$

where β_k is the weight given to the kth classifier C_k. Weighted linear fusion introduces a *Z*-score normalisation step to improve the generalisability of the technique. *Z*-score normalisation sets the mean and standard deviation of the score distribution to zero and unity, respectively. The normalisation provides a consistent frame of reference from which the scores can be fused and is made under the assumption that the scores are normally distributed. The scores with the same range of magnitude are achieved as the outputs of the normalisation. Two properties of *Z*-score normalisation are:

- the resultant client scores are displaced further from the imposter scores and
- there will be a reduction in the variance of the combined imposter scores.

Z-scored normalisation is performed before linear logistic regression (*llr)* algorithms are applied to provide a consistent frame of reference between the weights being derived.

The *llr* is chosen in this research because it has a convex cost function and so will converge to a solution. The cost functions for the *llr* make use of the logit function. The logit function is defined as

$$\text{logit}\,P = \log\frac{P}{1-P}. \tag{17}$$

The cost function of the *llr* is as follows,

$$C_{llr} = \frac{P}{K}\sum_{j=1}^{K}(1+e^{-f_j-\text{logit}P}) + \frac{1-P}{L}\sum_{j=1}^{L}\log(1+e^{g_j+\text{logit}P}). \tag{18}$$

For this cost function K is the number of true trials, L is the number of false trials, P is the synthetic prior (which by default is $P=0.5$) and the fused target and non-target scores are, respectively,

$$f_j = \alpha_0 + \sum_{i=1}^{N}\alpha_i s_{ij} \quad \text{and} \quad g_i = \alpha_0 + \sum_{i=1}^{N}\alpha_i r_{ij}. \tag{19}$$

A package provided by Brummer [37] is utilised for the implementation of this score fusion and the results of fusing the three classifiers together is provided in the following table.

It can be seen that the fusion of the Log-Gabor filter, DWT and DCT provides better performance than any individual classifier. The correct classification rate of good solder joint, excess solder joint and bridge solder joint improves to 98.5% followed by a classification rate of no solder joint which is 95%. The classification of less solder joint is increased from 60% to 70%. The average percentage of the correct classifications varies across different types from 98.5% to 70%. There are significant improvements in the EER also. An EER of less than 5% is achieved in most types of classification except for 6.5% of excess solder joint and 23% of no solder joint that are wrongly classified as less solder joint. 7% of less solder joint is wrongly classified as no solder joint. The total execution time for classification of one solder joint takes approximately 20–30 s depending on the size of the image and the processing speed of the computer. As a result, this system is able to be employed in real time manufacturing.

It was anticipated that fusion would lead to an improved classifier for classification of less solder joint; however, the results indicate that the linear fusion does not lead to improved classification. On the whole, a significant performance improvement is obtained. Scores from the three classifiers (i.e., Log-Gabor filter, DWT and DCT) are fused together to obtain the desired characteristics of the individual classifiers. The main features of the individual filter are as follows. The Log-Gabor filter appears to be a logical choice for the task of frequency partitioning while wavelet analysis provides a compact representation, which separates the frequency content of the image. In addition, the Discrete Cosine Transform is associated with compression tasks and its compactness and similarities to the Fourier transform make it well suited to this research. Furthermore, the correct classification percentage is high for the each type of feature mentioned above, and the features of the Log-Gabor filter achieve the highest percentage value overall. An advantage of the proposed approach is that this system does not need special positioning systems and hardware for acquisition of the image. This allows less expensive solutions in the implementation of the classification system than those methods that require complex illumination systems.

The proposed classifier achieves a high recognition rate with little overhead of computation. This proposed system does not need any special illumination system, and the images are acquired by a standard digital camera. In fact, the choice of suitable features allows overcoming the problem given by the use of non complex illumination systems while other inspection systems need complex image acquisition methods. Moreover, the use of the Log-Gabor filter and classifier fusion can overcome the limitation of neural networks, which have been applied to previous classification systems. This system achieves the correct classification percentage as high as other complex inspection systems. The physical parameters of industrial processes are not required to be included in the classification process and the five different types of solder joints are successfully classified depending on the quality of solder joints.

6. Conclusion

This paper has provided a solution to overcome some of the limitations of current optical inspection techniques and has proposed two inspection modules for an automatic solder joint classification system. The "front-end" inspection system proposed a novel illumination normalisation approach for solder joint segmentation. Illumination variations under different lighting conditions can be significantly reduced by discarding low-frequency DCT coefficients. This approach has advantages in: (1) no modelling steps are required and (2) this approach is fast and it can be easily implemented in a real-time solder joint segmentation system. The results show that this method can effectively eliminate the effects of uneven illumination and greatly improve the segmentation result.

The "back-end" inspection involves the classification of solder joints by using the Log-Gabor filter and classifier fusion. Five different levels of solder quality with respect to the amount of solder paste have been defined. The Log-Gabor filter was demonstrated to achieve high recognition rates and is resistant to misalignment. Further testing demonstrates the advantage of the Log-Gabor filter over both the Discrete Wavelet Transform and the Discrete Cosine Transform. Classifier score fusion was analysed for improving the recognition rate. The Classifier score fusion was approached as a linear score fusion since this method treats each source independently so that information from the sources can be maximised. Experimental results demonstrate that the proposed system improves performance and robustness in terms of classification rates. The performance of the preliminary inspection algorithms is encouraging; however, further improvements can be expected from the current technologies. More robust features could be developed by focusing on the errors of the current algorithm and the use of multiple views of solder joints could also improve classification performance.

Acknowledgements

The authors wish to acknowledge the kind cooperation of Mr. Ahmed Nabil Belbachir for providing Image database 1 utilised in this work.

References

[1] Loh HH, Lu MS. Printed circuit board inspection using image analysis. IEEE Transactions on Industry Applications 1999;35:426–32.
[2] Lee ZS, Lo RC. Application of vision image cooperated with multi-light sources to recognition of solder joints of PCB. TAAI artificial intelligence and applications; 2002. p. 425–30.
[3] Yang FC, Kuo CH, Wing JJ, Yang CK. Reconstructing the 3D solder paste surface model using image processing and artificial neural network. In: Proceedings of the IEEE international conference on systems, man and cybernetics; 2004. p. 3051–6.
[4] Lin SC, ChouCH, Su CH. A development of visual inspection system for surface mounted devices on printed circuit board. In: Proceedings of the 33rd annual conference of the IEEE industrial electronics society; 2007. p. 2440–5.

[5] Kim JH, Cho HS, Kim S. Pattern classification of solder joint images using a correlation neural network. Engineering Applications of Artificial Intelligence 1996;9:655–69.
[6] Jiang BC, Wang CC, Hsu YN. Machine vision and background remover-based approach for PCB solder joints inspection. International Journal of Production Research 2007;45:451–64.
[7] Bartlett SL, Besl PJ, Cole CL, Jain R, Mukherjee D, Skifstad KD. Automatic solder joint inspection. IEEE Transactions on Pattern Analysis and Machine Intelligence 1988;10:31–43.
[8] Capson DW, Eng SK. A tiered-color illumination approach for machine inspection of solder joints. IEEE Transactions on Pattern Analysis and Machine Intelligence 1988;10:387–93.
[9] Kim TH, Cho TH, Moon YS, Park SH. Visual inspection system for the classification of solder joints. Pattern Recognition 1999;32:565–75.
[10] Chiu SN, Perng MH. Reflection-area-based feature descriptor for solder joint inspection. Machine Vision and Applications 2007;18:95–106.
[11] Ong T, Samad Z, Ratnam M. Solder joint inspection with multi-angle imaging and an artificial neural network. The International Journal of Advanced Manufacturing Technology 2008;38:455–62.
[12] Belbachir AN, Lera M, Fanni A, Montisci A. An automatic optical inspection system for the diagnosis of printed circuits based on neural networks. In: Proceedings of the 40th IEEE industry applications society annual meeting; 2005. p. 680–4.
[13] Park JS, Tou JT. A solder joint inspection system for automated printed circuit board manufacturing. In: Proceedings of the IEEE international conference on robotics and automation, vol. 2; 1990. p. 1290–5.
[14] Kim JH, Cho HS. Neural network-based inspection of solder joints using a circular illumination. Image and Vision Computing 1995;13:479–90.
[15] Ko KW, Cho HS. Solder joints inspection using a neural network and fuzzy rule-based classification method. IEEE Transactions on Electronics Packaging Manufacturing 2000;23:93–103.
[16] Acciani G, Brunetti G, Fornarelli G. Application of neural networks in optical inspection and classification of solder joints in surface mount technology. IEEE Transactions on Industrial Informatics 2006;2:200–9.
[17] Acciani G, Brunetti G, Fornarelli G. A multiple neural network system to classify solder joints on integrated circuits. International Journal of Computational Intelligence Research 2006;2:337–48.
[18] Luo B, Zhang Y, Yu G, Zhou X. ANN ensembles based machine vision inspection for solder joints. In: Proceedings IEEE international conference on control and automation; 2007. p. 3111–5.
[19] Yun TS, Sim KJ, Kim HJ. Support vector machine-based inspection of solder joints using circular illumination. Electronics Letters 2000;36:949–51.
[20] Chen W, Er MJ, Wu S. Illumination compensation and normalization for robust face recognition using discrete cosine transform in logarithm domain. IEEE Transactions on Systems Man, and Cybernetics—Part B 2006;36: 458–66.
[21] MathWorks_Inc.. Matlab, the language of technical computing.
[22] Al-Nu'aimi AA, Qahwaji R. Digital colored image watermarking using YIQ color format indiscrete wavelet transform domain; 2006.
[23] Ridler TW, Calvard S. Picture thresholding using an iterative selection method. IEEE Transactions on Systems Man and Cybernetics 1978;8:630–2.
[24] Gonzalez RC, Woods RE. Digital image processing. 2nd ed. Pearson: Prentice Hall; 2002.
[25] Frew E, Huster A, LeMaster E. Image thresholding for object detection. 1997.
[27] Cook J, McCool C, Chandran V, Sridharan S. Combined 2D/3D face recognition using log-gabor templates. In: Proceedings of the IEEE international conference on video and signal based surveillance; 2006. p. 83–8.
[28] Mar NSS, Fookes C, Yarlagadda PKDV. Automatic solder joint defect classification using the Log-Gabor filter. Advanced Materials Research 2009;97–101:2940–3.
[29] Ibrahim Z, Al-Attas SAR, Aspar Z, Mokji MM. Performance evaluation of wavelet-based PCB defect detection and localization algorithm. In: Proceedings of the IEEE international conference on industrial technology, vol. 1; 2002. p. 226–31.
[30] Daugman J. Two-dimensional spectral analysis of cortical receptive field profiles. Vision Research 1980;20:847–56.
[31] Field DJ. Relations between the statistics of natural images and the response properties of cortical cells. Journal of Optical Society of America 1987;4:2379–94.
[32] Cook JA, Decompositional A. Investigation of 3D face recognition. Brisbane, Australia: Queensland University of Technology; 2007.
[33] Lucey S., Chen T.. Face recognition through mismatch driven representations of the face. In: Proceedings of the 2nd joint IEEE international workshop on visual surveillance and performance evaluation of tracking and surveillance, 2005, p. 193–9.
[34] Sanderson C, Paliwal KK. Fast features for face authentication under illumination direction changes. Pattern Recognition Letters 2003;24:2409–19.
[35] Eickeler S, Müller S, Rigoll G. Recognition of JPEG compressed face images based on statistical methods. Image and Vision Computing 2000;18:279–87.
[36] Mokju M, Abu-BakarSAR. Fingerprint matching based on directional image constructed using expanded Haar wavelet transform. In: Proceedings of the international conference on computer graphics, imaging and visualization; 2004. p. 149–52.
[37] Brummer N. Tools for fusion and calibration of automatic speaker detection systems. Retrieved from 〈http://www.dsp.sun.ac.za/.nbrummer/focal/index.htm〉.
[38] Stefano LD, Boland F. A new phase extraction algorithm for phase profilometry. Machine Vision and Applications 1997;10:188–200.